文章编号:1006-9941(2020)09-0925-11

Characterization and Thermochemical Properties of NC/GAP/nano-TATB Electrospinning Composite Fibers with 3D Network Structure

LUO Ting-ting[1], **WANG Yi**[1*], **LIU Li-xia**[2], **SONG Xiao-lan**[3]

(1.*School of Materials Science and Engineering, North University of China, Taiyuan* 030051, *China*; 2. *North Blasting Technology Co., Ltd., Yangquan Branch, Yangquan* 045000, *China*; 3. *School of Environment and Safety Engineering, North University of China, Taiyuan* 030051, *China*)

Abstract: A composite fiber nitrocellulose/glycidyl azide polymer/nanometer 1, 3, 5-triamino-2, 4, 6-trinitrobenzene (NC/GAP/nano-TATB) with three-dimensional structure was prepared by electrospinning method. Differential scanning calorimeter (DSC) and online thermal-infrared spectrometry (TG-IR) measurement were conducted to probe the low temperature thermochemical properties of the composite fiber. Result indicates that there is only one exothermic peak existing in its DSC curve, which means that NC, GAP, and nano-TATB decomposed simultaneously rather than decomposed individually. The activation energy (E_a) of NC/GAP/nano-TATB (208.1 kJ·mol^{-1}) is lower than nano-TATB (228.9 kJ·mol^{-1}), and the rate constant (k) of NC/GAP/nano-TATB (1.70 s^{-1}) is higher than nano-TATB (0.92 s^{-1}). The composite fiber is easier to be activated and will decompose faster than nano-TATB. The main products for thermal decomposition of NC/GAP/nano-TATB include CO_2, N_2O, NO, CO, NO_2 and H_2O, meanwhile, fragments like —CH—, —CH_2O, and C—O—C were also detected. Moreover, the energetic performance and sensitivity of the composite fiber have been detailedly evaluated and compared with that of NC/GAP and nano-TATB. Combustion temperature (T_c) of NC/GAP/nano-TATB is up to 1583 ℃ and the addition of nano-TATB is favorable to the reduction of impact sensitivity.

Key words: electrospinning; NC/GAP/nano-TATB; thermal decomposition; energetic performance; sensitivity

CLC number: TJ55; O649 **Document code**: A **DOI**: 10.11943/CJEM2019283

1 Introduction

Energetic materials are extensively used in various weapon systems[1-3]. With the development of modern weapons, energetic materials need to be further improved, including higher density, higher reactivity, lower sensitivity, higher burning rate and higher specific impulse[4-6]. For the same energetic material, compared with coarse size energetic materials, nano-scale energetic materials have excellent properties such as high reaction rate and low sensitivity. This is attributed to the intimated contact of the particles[7-9]. However, due to high surface energy, energetic nanoparticles are easily agglomerated. Energetic nanocomposites draw attention of researchers, which consists of a nano-matrix with energetic nanoparticles loading on it. This nano-matrix can effectively hinder the agglomeration of nanoparticles[10-13]. Nano-TATB has features of high energy performance, smaller critical diameter, faster and more stable detonation wave propagation, in addition to retaining low sensitivity and high thermostability. Hence, nano-TATB is a significant component of energetic nanocomposites.

In recent years, electrospinning technology has been introduced to the fabrication of nanocomposites. Its products, i.e. nanofiber, have net-like structures with high specific surface area, which are ide-

Received Date: 2019-11-06; **Revised Date**: 2020-02-20

Published Online: 2020-06-11

Project Supported: Weapons and Equipment Pre-research Fund

Biography: LUO Ting-ting (1994-), female, master degree candidate, research direction: solid propellants.

e-mail: luotingting1002@163.com

Corresponding author: WANG Yi (1980-), male, associate professor, research direction: solid propellants.

e-mail: wangyi528528@aliyun.com

引用本文:罗婷婷,王毅,刘丽霞,等. 3D网状静电纺NC/GAP/nano-TATB纤维的表征及热化学性能[J]. 含能材料,2020,28(9):925-935.

LUO Ting-ting, WANG Yi, LIU Li-xia, et al. Characterization and Thermochemical Properties of NC/GAP/nano-TATB Electrospinning Composite Fibers with 3D Network Structure[J]. *Chinese Journal of Energetic Materials (Hanneng Cailiao)*, 2020, 28(9):925-935.

al carriers for loading nanoparticles[14-21]. However, only a few studies are conducted concerning the application of electrospinning in the field of energetic nanocomposites. For example, Yan[22] obtained nitrocellulose/aluminum-cupric oxide (NC/Al-CuO) nanofibers with high burning rate. Nanoboron/nitrocellulose (B/NC) and nitrocellulose/2, 4, 6, 8, 10, 12-hexanitro-2, 4, 6, 8, 10, 12-hexaazaisowurtzitane (NC/CL-20) nanofibers were prepared based on electrospinning methed, and these nanofibers also burned violently[23-24]. All of them choose NC as the martix of electrospun. In fact, in previous attempts, we have employed NC as the precusor to fabricate nanofibers loaded with explosive nanoparticles. It has been found that the rather high viscosity of the NC solution results in a quite low load of explosive nanoparticles and high electrospinning voltage. In this sense, if you want to increase the load, it is indispensable to lower the viscosity of the precusor solution. Decreasing the concentration of NC will lead to a penalty in the structure of nanofibers. In this regard, using or introducing a precusor with low viscosity may be a good choice in the case of a composite nanofiber with high load of explosive nanoparticles. GAP is an energetic prepolymer with low viscosity and high energy[25]. Meanwhile, it has remarkably lower glass transition temperature (T_g) and higher density than NC[26]. At present, no attempt has been made that involves using GAP as a precusor to fabricate nanofibers with electrospun. In the present paper, partial NC is replaced by GAP to reduce the viscosity of electrospinning solution. Meanwhile, the safety problems caused by high electrospinning voltage can be avoided effectively. The TATB nanoparticles are loaded on the composite matrix of NC/GAP by an electrospinning method to obtain a NC/GAP/nano-TATB nanofiber. Analyses such as SEM, EDS, XRD, IR, and XPS are employed to investigate the morphology structures of samples. DSC and TG-IR analyses are conducted to probe the low temperature thermochemical properties of the composite fiber. The energy performance of the NC/GAP/nano-TATB nanofibers are analyzed from the perspective of the formation enthalpy (ΔH_f), oxygen balance (OB), and C/H mass ratio.

2 Experimental

2.1 Materials

Nitrocellulose(NC, 12.6% N, industrial grade) is purchased from Foshan Junyuan Chemical Co., Ltd (Foshan, China). Glycidylazide polymer (GAP, M_n=4000, hydroxyl value of 0.49 mmol·g^{-1}) is provided by the 42nd Institute of the Fourth Academy of China Aerosce Science and Technology Corporation. Raw TATB is purchased from Gansu Yinguang Chemical Co., Ltd (Baiyin, China). Ethanol (EtOH) and acetone are purchased from Tianjin Guangfu Chemical Co., Ltd (Tianjin, China).

2.2 Preparation of NC/GAP/nano-TATB nanofiber

Nano-TATB is obtained by the ball milling method. The ingredients, including 200 g balls, 6 g TATB, 60 mL water and 60 mL EtOH, are added into a mill jar. The jar is sealed and fixed on the ball mill. The planet carrier rotates at 350 r·min^{-1} for 6 h. The TATB nanoparticles are separated from the suspension and are dehumidified by freeze drying.

NC/GAP/nano-TATB nanofiber is prepared as follows. The mass ratio of NC, GAP, and nano-TATB is set to 3∶3∶2. Firstly, the nano-TATB suspension is prepared by dispersing 0.3 g nano-TATB into 4.4 g acetone, and the NC/GAP solution is obtained via dissolving 0.45 g NC and 0.45 g GAP into 4.4 g acetone. Then, the above-synthesized nano-TATB suspension and NC/GAP solution are mixed to get a NC/GAP/nano-TATB precursor solution (12%). For the electrospinning process, the inner diameter of the stainless steel needle is 0.8 mm. Moreover, the flow rate is 4-6 mL·h^{-1}, and the applied voltage is fixed at 12−18 kV. The collection distance is 12 cm. Eventually, the electrospun nanofibers deposit on the aluminum foil. The preparation scheme of NC/GAP/nano-TATB is described in Fig.1.

For contrast experiment, the NC/GAP precursor solution (12%) is synthesized by dissolving 0.6 g NC and 0.6 g GAP into 8.8 g acetone. The electros-

pinning process of NC/GAP is the same as that of NC/GAP/nano-TATB nanofiber.

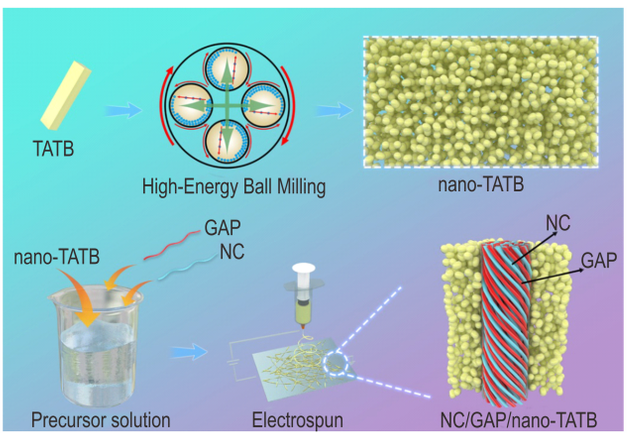

Fig.1 Sketch for the synthesis of NC/GAP/nano-TATB composite nanofiber

2.3 Characterization

The morphologies of nanofiber and nano-TATB are observed by a scanning electron microscope (SEM, Hitachi SU8010). The X-ray diffraction (XRD) analysis is performed on a DX-2700 X-ray diffractometer (Haoyuan) with CuK_{α} radiation. IR spectrum is obtained on an infrared spectrometer (American Thermo Fisher Scientific Nicolet 6700). XPS is conducted with X-ray photoelectron spectroscopy (XPS) and a PHI5000 Versa-Probe (ULVAC-PHI). The BET measurements are performed utilizing the nitrogen adsorption with Micromeritics ASAP 2010 instrument. Thermal analysis is conducted on a differential scanning calorimeter (DSC, TA Model Q600) at heating rates of 5, 10, 15 ℃·min^{-1} and 20 ℃·min^{-1}. TG-IR analysis is performed on a thermal analyzer system (TG/DSC, Mettler Toledo) coupled with a Fourier transform infrared spectrometer in nitrogen atmosphere. The impact sensitivity is detected using an HGZ-1 impact equipment and referring to the method in GJB772A-97. The drop ball used in the test is 2.5 kg, and the dosage is (35±1) mg each time. Each sample is tested 25 times.

3 Results and Discussion

3.1 Morphology and structure

As is shown in Fig.2a, the nano-TATB presents the micron morpholgy of ellipsoid. The particles diameter distribution of nano-TATB are calculated via measuring a diameter of ~100 particles, and the results are shown in Fig.2b. The mean diameter calculated by the frequency curve is 133.3 nm. Fig. 3 shows that the NC/GAP and NC/GAP/nano-TATB nanofbers both keep three-dimensional reticulation morphologies. Form Fig.3a, the surface of NC/GAP is smooth and uniform. With Fig.3b in comparison, the nano-TATB is entrapped on the surface of the NC/GAP nanofibers, and the surface morphology of NC/GAP/nano-TATB is rough and inhomogenous. This distinction is put down to the factors that the addition of nano-TATB makes the NC/GAP/nano-TATB precursor solution not as homogeneous as the pure NC/GAP solution. In addition, it is probably caused by the aggregation of nano-TATB. For the NC/GAP nanofibers, the mean diameter are 469 nm. For the NC/GAP/nano-TATB nanofibers, the mean diameter is 1036 nm. It is evident that the diameter of NC/GAP/nano-TATB is larger than that of NC/GAP, which is beacause there are TATB nanoparticles incorporating on the surface of NC/GAP.

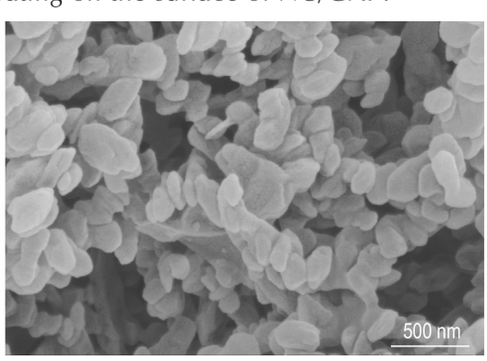

a. SEM image of TATB nanoparticles

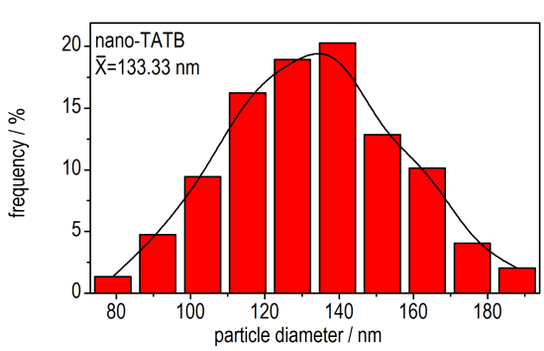

b. diameter distribution of the TATB nanoparticls

Fig.2 Morphology analysis of TATB

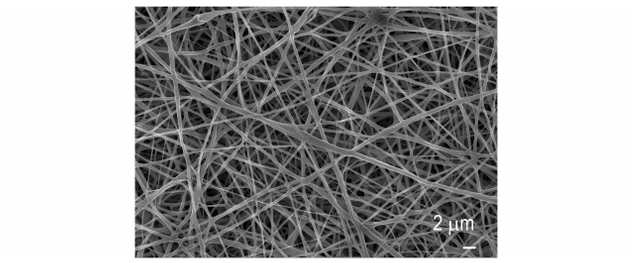

a. SEM image of NC/GAP

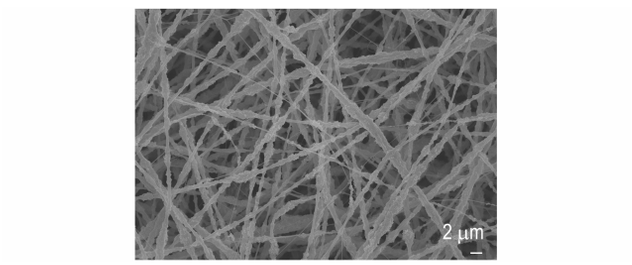

b. SEM image of NC/GAP/nano-TATB

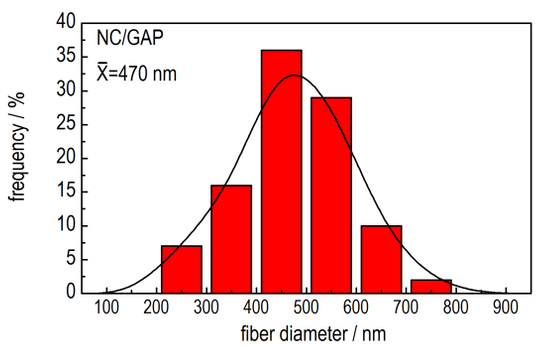

c. diameter distribution of NC/GAP

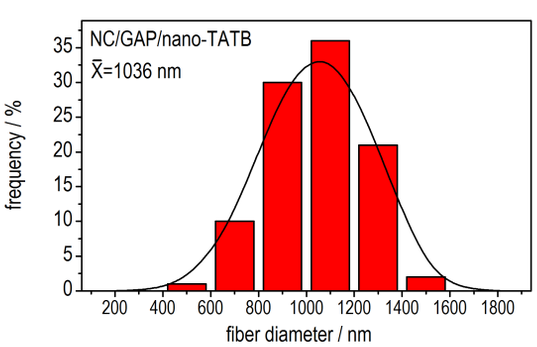

d. diameter distribution of NC/GAP/nano-TATB

Fig.3 Morphology analysis of fibers

The EDS spectrograms of NC/GAP and NC/GAP/nano-TATB are illustrated in Fig. 4. It can be found that only the characteristic peaks of C, N and O elements appear. The calculation results of detailed elements content for NC/GAP and NC/GAP/nano-TATB are listed in Table 1. It is confirmed that after coating nano-TATB, there is no change in O content, N content significantly increases and C content declines.

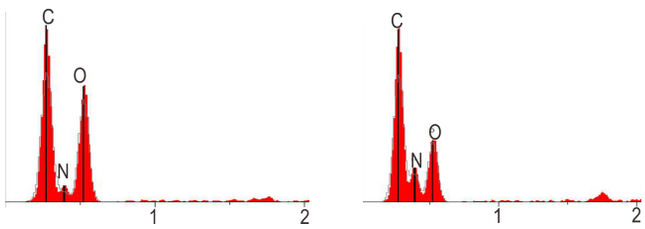

a. NC/GAP **b.** NC/GAP/nano-TATB

Fig.4 EDS spectra of samples

Table 1 Theoretical element contents of EDS analysis

Sample	C	N	O
NC/GAP	31.45	27.3	37.2
NC/GAP/nano-TATB	30.6	28.8	37.2

To illustrate the surface groups of the NC/GAP/nano-TATB nanofibers, IR analyses of samples are conducted, and the IR spectra are dispalyed in Fig.5. For the NC/GAP nanofibers, two absorption peaks situated at 1280 cm^{-1} and 1650 cm^{-1} represent the symmetric and anti-symmetric stretching vibrations of $—ONO_2$. The peaks at 1068 cm^{-1} and 848 cm^{-1} refer to the inter-ring stretching vibrations of C—O and C—O—NO_2 deformation vibrations. All these vibrations match with the molecular structure of NC[27]. The peak at 2100 cm^{-1} reflects the stretching vibrations of $—N_3$ in GAP[28]. In light of nano-TATB, the peaks at 3310 cm^{-1} and 3213cm^{-1} refer to the symmetric and anti-symmetric stretching vibrations of Ar—NH_2, respectively. The peaks at 1613, 1561 cm^{-1}, and 1438 cm^{-1} indicate the stretching vibrations of the C=C skeleton in the benzene ring. Two strong absorption peaks located at 1221 cm^{-1} and 1174 cm^{-1} correspond to the symmetric and antisymmetric stretching vibrations of Ar—NO_2[29]. All these peaks in NC/GAP and nano-TATB also exist in the spectrum of NC/GAP/nano-TATB. The XRD patterns of samples are shown in Fig.6. NC/GAP is an energetic polymer. Hense, there are only dispersion peak in the pattern of NC/GAP. Nano-TATB shows characteristic peaks at 28.36° and 42.27°, where the peaks of NC/GAP/nano-TATB also occur.

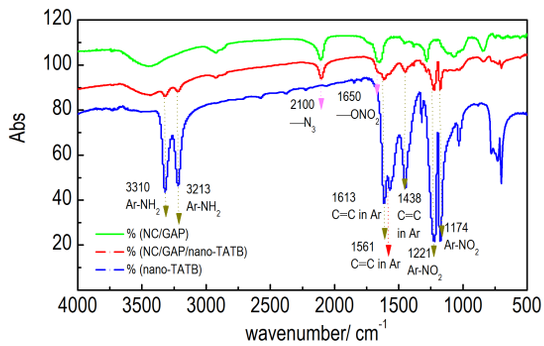

Fig.5 IR patterns of sample

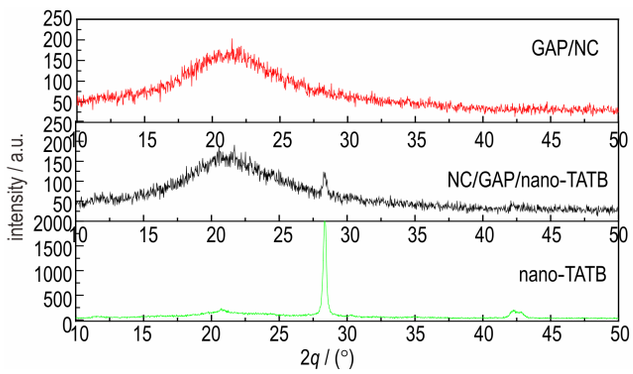

Fig.6 XRD patterns of samples

For the NC/GAP/nano-TATB nanofibers, the chemical states of surface elements are further investigated by XPS. Fig. 7a shows that the nanofibers are composed of carbon, nitrogen and oxygen elements. The high-resolution XPS spectra of C, N and O elements are exhibited in Fig.7b-7d. The O 1s spectra is fitted to four peaks. The peak at 532.5 eV relates to — NO_2 in TATB[30]. The peaks at 533.5 eV and 534.2 eV belong to —O*—NO_2 and —O—NO*$_2$ in NC[31]. The peak at 531.4 eV is ascribed to the C—O group in NC and GAP. The C 1s spectrum presents three features binding energies of 284.3, 286.3 eV and 288.4 eV corresponding to C—C, C—N, and C—O, respectively. The XPS spectrum of N 1s consists of four peaks at 399.3, 400.4, 404.0 eV, and 407.5 eV, which are assigned to — NH_2, — N_3, — NO_2 and — ONO_2[32]. The — N_3 and — ONO_2 groups imply the presence of GAP and NC in the nanofibers. The groups of — NH_2 and — NO_2 belong to TATB, which illustrates the loading of nano-TATB on the surface of NC/GAP.

The Nitrogen adsorption-desorption isotherms of the NC/GAP and NC/GAP/nano-TATB nanofibers are shown in Fig.8. And the BET specific surface areas, pore volumes and pore sizes of the nanofibers

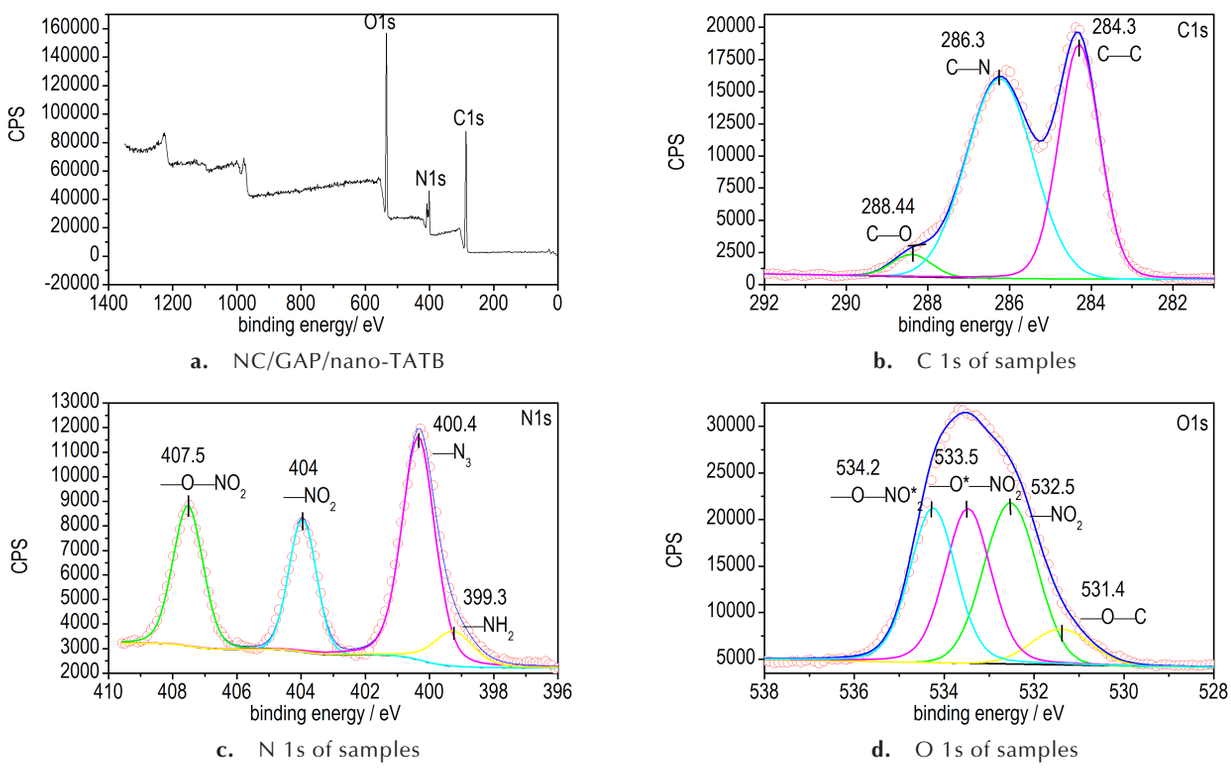

Fig.7 XPS spectra of of samples

are listed in Table 2. From Fig.8, the isotherms are regarded as class IV (H3-type hysteresis loop), corresponding to the mesoporous material[33]. The inflection point B usually corresponds to the completion of the single layer adsorption, which is initially similar to the adsorption process of macroporous materials. The capillary condensation causes the sharp rise of adsorption. Capillary condensation and capillary evaporation generally do not occur under the same p/p^o, which leads to the creation of hysteresis loops[34]. The surface area of the NC/GAP nanofibers (4.3573 $m^2 \cdot g^{-1}$) is larger than that of the NC/GAP/nano-TATB nanofibers (4.2331 $m^2 \cdot g^{-1}$). It results from the lower diameter of NC/GAP nanofibers.

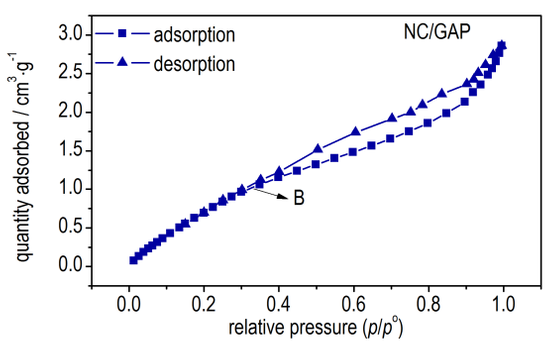

a. NC/GAP nanofibers

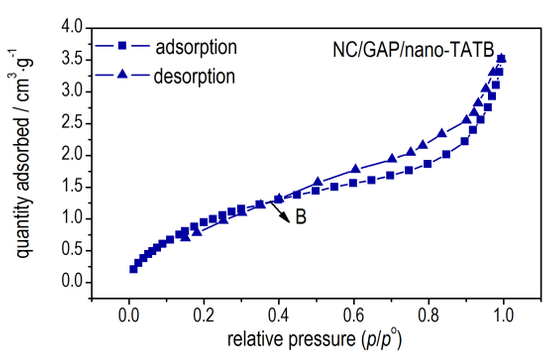

b. NC/GAP/nano-TATB nanofibers

Fig.8 The BET data of samples

Table 2 BET surface area and pore structure parameters of nanofibers

sapmles	bet surface area/$m^2 \cdot g^{-1}$	pore volume /$cm^3 \cdot g^{-1}$	pore size /nm
NC/GAP	4.3573	0.004422	4.05911
NC/GAP/nano-TATB	4.2331	0.005440	5.14075

3.2 Thermal analysis

The DSC curves of NC/GAP, nano-TATB and NC/GAP/nano-TATB collected at different heating rates are displayed in Fig.9, and they are utilized to calculate the kinetic and thermodynamic parameters in Table 3. For all samples, the exothermic peak temperature increases with the increase of heating rate. For NC/GAP and nano-TATB, there is only one exothermic peak. In regard to the NC/GAP/nano-TATB nanofibers, at the heating rate of 5 ℃·min^{-1}, there are two exothermic peaks in DSC curve. However, as the heating rate increases to 10, 15 ℃·min^{-1}, and 20 ℃·min^{-1}, only one peak exists. This means that they decompose simultaneously at high heating rates. The thermal decomposition rate of NC/GAP/nano-TATB is significantly higher than those of NC/GAP and nano-TATB. In addition, the exothermic peak temperature of the NC/GAP/nano-TATB nanofibers is markedly lower than those of the NC/GAP nanofibers and nano-TATB, which indicates that NC, GAP and nano-TATB provide synergistic effects for the thermal decomposition. This might be due to that the nanofibers with large specific surface area possess excellent thermal conductivity and heat mass transfer properties.

The Activation energy (E_a), pre-exponential factor (A_K), and rate constant (k) are calculated with Kissinger equation (Eqs.(1)) and Arrhenius equation (Eqs.(2))[35]. The E_a of NC/GAP/nano-TATB is 208.124 kJ·mol^{-1}, which is higher than that of NC/GAP and is lower than that of nano-TATB. The introduction of nano-TATB facilitates the activation of nanofibers. The k of NC/GAP/nano-TATB is hgher than that of nano-TATB and NC/GAP, demonstrating that the thermal decomposition of NC/GAP/nano-TATB is faster than that of NC/GAP and nano-TATB.

The essence of thermal decomposition is the activation and fracture of the explosive molecular bonds. When the explosive molecules are heated, the molecular thermal motion intensifies. At the critical temperature, the weakest bonds are stretched. When stretching to the limit, the fracture of the weakest bonds occur, accompanying with a change in energy. The activation process of explosives is an

endothermic process, which is depicted by the thermodynamic parameters of $\Delta G^{\neq}$ (free energy of activation), $\Delta H^{\neq}$ (enthalpy activation), and $\Delta S^{\neq}$ (entropy of activation) calculated via Eqs.(3)−(5). $\Delta G^{\neq}$ means the chemical potential of the explosive molecule in the activation reaction, whose values are positive numbers. This signifies that all of activation processes are non-spontaneou[36]. Hence, the explosives remain steady under normal conditions. $\Delta H^{\neq}$ represents the required energy of molecular activation, which is similar to the definition of E_a. The kinetic compensation effect for the thermolysis of NC/GAP, nano-TATB and NC/GAP/nano-TATB are displayed in Fig. 9e. It is clear that the points of NC/GAP, NC/GAP/nano-TATB and nano-TATB do not present a linear relationships. This implies that the three samples have disparate decomposition mechanisms in kinetics.

$$\ln\frac{\beta}{T_p} = \ln\frac{R \cdot A_k}{E_a} - \frac{E_a}{R}\cdot\frac{1}{T_p} \tag{1}$$

$$k = A_k \cdot \mathrm{Exp}\left(-\frac{E_a}{T_p \cdot R}\right) \tag{2}$$

$$A\exp\left(-\frac{E_a}{RT_p}\right) = \frac{K_B T_P}{h}\exp\left(-\frac{\Delta G^{\neq}}{RT_P}\right) \tag{3}$$

$$\Delta H^{\neq} = E_a - RT_P \tag{4}$$

$$\Delta G^{\neq} = \Delta H^{\neq} - T_P \Delta S^{\neq} \tag{5}$$

where T_p is the peak temperature in the DSC trace with a heating rate of 15 ℃·min^{-1}; K_B and h are the Boltzmann (K_B=1.381×10^{-23} J·K^{-1}) and Planck constants (h=6.626 × 10^{-34} J/s), respectively; β is the heating rate.

With regard to the NC/GAP/nano-TATB nanofi-

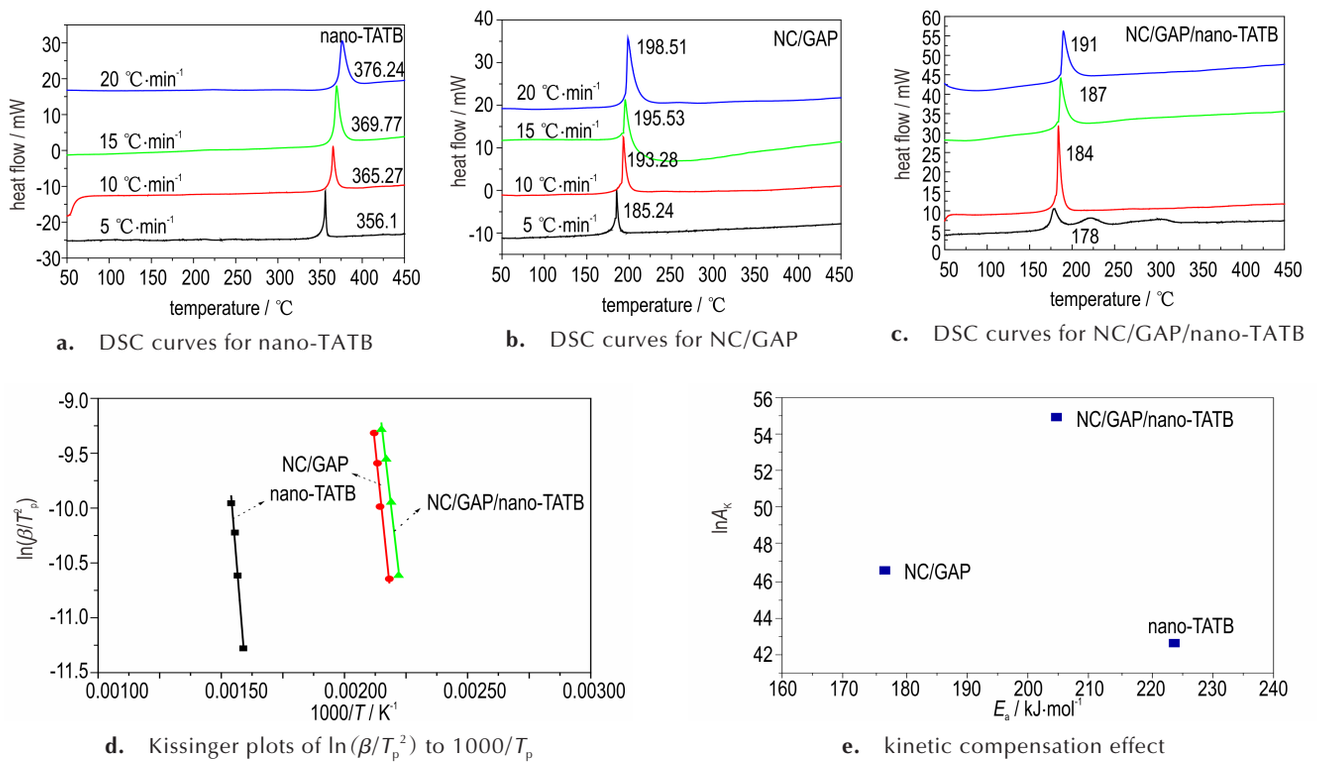

a. DSC curves for nano-TATB **b.** DSC curves for NC/GAP **c.** DSC curves for NC/GAP/nano-TATB

d. Kissinger plots of $\ln(\beta/T_p^2)$ to $1000/T_p$ **e.** kinetic compensation effect

Fig.9 Thermal decomposition analysis of samples

Table 3 Thermodynamics and kinetics deduced from DSC traces

Samples	T_p /K	Thermodynamics			Kinetics		
		$\Delta H^{\neq}$/kJ·mol^{-1}	$\Delta G^{\neq}$/kJ·mol^{-1}	$\Delta S^{\neq}$/J·mol^{-1}·K^{-1}	E_a/kJ·mol^{-1}	lnA_K	k /s^{-1}
Nano-TATB	642.92	223.564	162.012	95.74	228.909	42.74	0.92
NC/GAP	468.68	176.242	115.152	130.345	180.139	46.59	1.431
NC/GAP/nano-TATB	459.76	204.302	112.228	201.581	208.124	54.98	1.70

bers, the products and mechanism of thermal decomposition are assessed by TG-IR. The TG and DTG curves are exhibited in Fig.10a, and the IR patterns intercepted at different temperature are displayed in Fig.10b. From Fig.10a, the incipient decomposition temperature of NC/GAP/nano-TATB is about 198 ℃. The decomposition rate reaches its maximum value at point of 203 ℃ and the decomposition is accomplished at 214 ℃. In Fig.10b, at 3740 cm^{-1} and 1556−1610 cm^{-1}, the peaks correspond to H_2O and NO_2. At 1182−1185 cm^{-1}, the peak reflects the fragments of —C—O—C—. The peak at 2116−2201 cm^{-1} represents the generation of CO. The peak at 1883−1924 cm^{-1} indicates the presence of NO. The existence of CO_2 explains the peak located at 2311−2361 cm^{-1}. The peaks at 1664−1794 cm^{-1} and 3230−3331 cm^{-1} are in accordance with the $—CH_2O$ and —CH debris, respectively. The $—ONO_2$ is the energetic group of NC, and the energetic groups of TATB are $—NO_2$ and $—NH_2$. The $·NO_2$ radical reacts with $—NH_2$ and —C to produce N_2O, NO_2, NO, CO and CO_2[37].

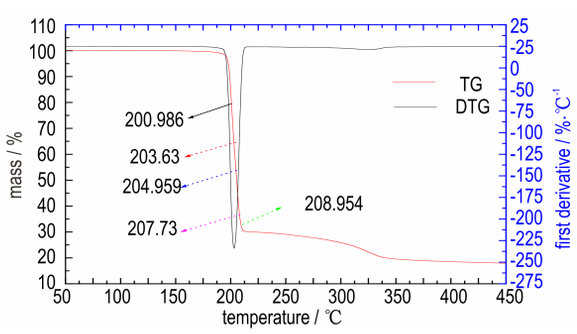

a. TG and DTG curves

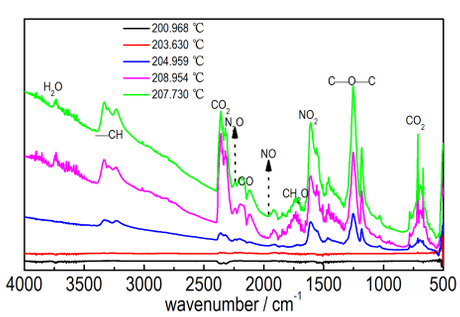

b. IR spectra of decomposition products at different temperatures

Fig.10 TG-IR analysis of samples

The $—N_3$ group, which is the energetic group of GAP, decomposes to N_2. N_2 has no infrared absorption and can not be probed by IR. The signal of CO is relatively strong, which is due to the large negative oxygen balance coefficient of NC/GAP/nano-TATB.

3.3 Energy properties and sensitivities

To explore the energy properties of NC/GAP/nano-TATB, the impact sensitivities and energy performances of the samples are tested. The standard specific impulse(I_{sp}), characteristic velocity (C^*), combustion chamber temperature(T_c) and average molecular mass of combustion products (M_c) are calculated and the results are listed in Table 4. Meanwhile, the combustion products and their molar ratios are also calculated, and the results are shown in Fig.12. Moreover, the speciality height (H_{50}), characterizing the impact sensitivity of samples, are tested and listed in Table 4. Obviously, the addition of nano-TATB brings about an evident decrease of H_{50} for NC/GAP, indicating that the NC/GAP/nano-TATB nanofibers possess lower sensitivity than NC/GAP. For energy performance, the I_{sp} of NC/GAP/nano-TATB and NC/GAP propellant are 2000.9 N·s·kg^{-1} and 2013.8 N·s·kg^{-1}, respectively. This phenomenon is associated with the formation enthalpy (ΔH_f), oxygen balance (OB), and C/H mass ratio of the samples. The working course of propellant is an effective transformation process to convert chemical energy into heat energy and transform heat energy into kinetic energy by acting[37−38]. Hence, chemical energy storage and energy conversion efficiency are crucial factors to energy performance. The former is represented by T_c, which is relevant to formation enthalpy (ΔH_f), oxygen balance (OB) and C/H mass ratio. As formation enthalpy(ΔH_f), oxygen balance(OB) and C/H mass ratio increase, the value of T_c increases. The formation enthalpy of nano-TATB is −139.75 kJ·mol^{-1}, which is observably larger than that of NC/GAP (−294.6 kJ·mol^{-1}). The C/H value of nano-TATB (8.6) is higher than the C/H value of NC/GAP(8.1). The(OB) of NC/GAP and nano-TATB are −76.1 and −55.78, respectively. Hence, the addition of nano-TATB is beneficial to the increase of chemical en-

ergy storage for NC/GAP. Fig.11c shows that combustion chamber temperature (T_c) improves with the mass percent of TATB increasing. The energy conversion efficiency is inversely proportional to M_c. The reduction of hydrogen content causes that H_2 ratio in combustion products decreases and M_c increases. The hydrogen content of TATB is lower than that of NC/GAP. As is shown in Fig.11d, the value of M_c enhances with the increasing of TATB. Fig.12 shows that the H_2 molar ratio for TATB(21%) is lower than NC/GAP(28%). The incorporation of TATB leads to a decrease of energy conversion efficiency for NC/GAP. In this case, in spite of higher T_c of TATB, the TATB has lower I_{sp} than NC/GAP. It is because the high storage of chemical energy of TATB is counteracted by the negative effect of low energy conversion efficiency. Hence, the interposition of TATB slightly reduces the energy performance of NC/GAP.

Table 4 Impact sensitivity and energy performance of samples

Samples	Impact sensitivity	Energy performance			
	H_{50}/cm	I_{sp}/N·s·kg^{-1}	C^*/m·s^{-1}	T_c/K	M_c
NC/GAP(50/50)	59.28	2013.8	1239.9	1556	22.296
TATB(100)	>100	1963.7	1216.1	1695	24.446
NC/GAP/TATB(37.5/37.5/25)	90.87	2000.9	1233.2	1583	22.788

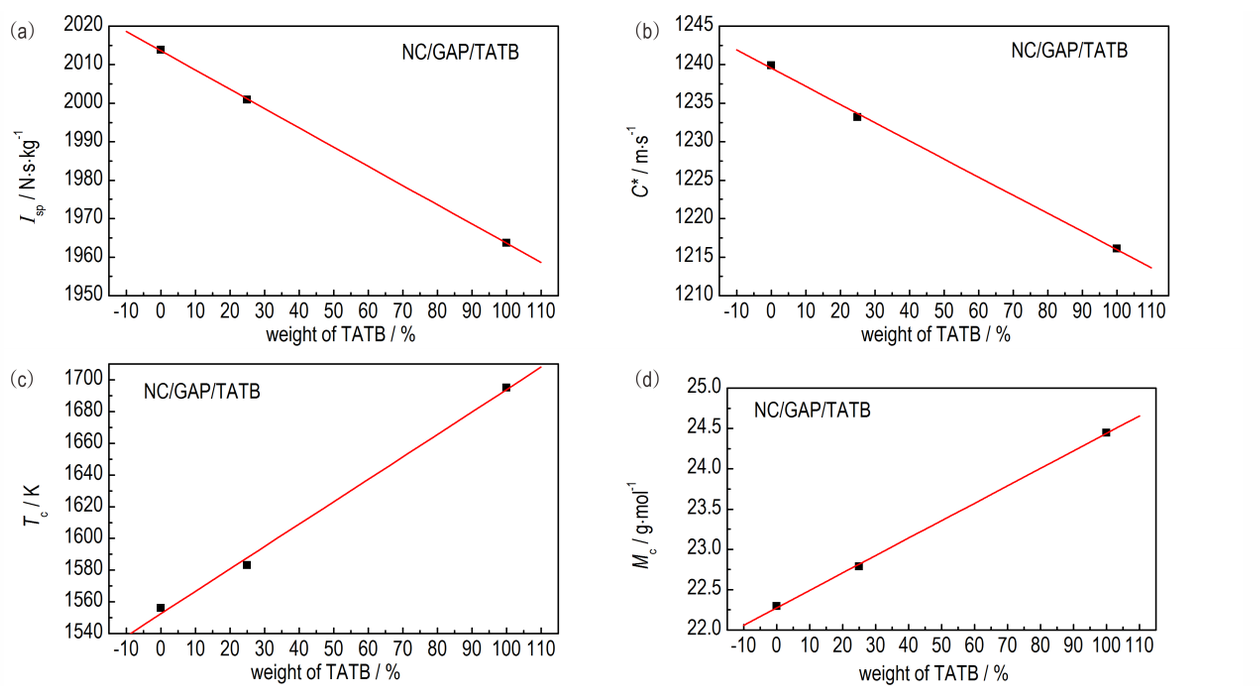

Fig.11 Energy performances of NC/GAP/TATB nanofibers as a function of mass percentage of TATB

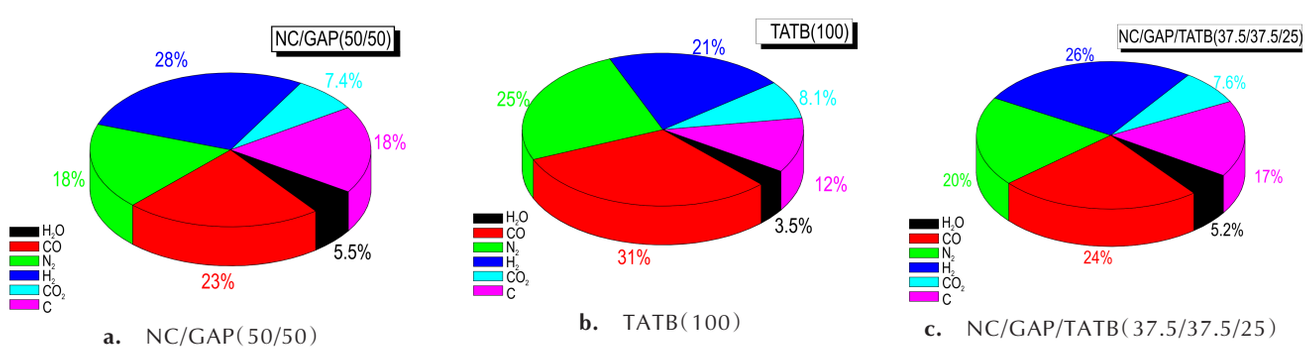

a. NC/GAP(50/50) **b.** TATB(100) **c.** NC/GAP/TATB(37.5/37.5/25)

Fig.12 Combustion products and their molar ratios

I_{sp} is Standard specific impulse; C^* is Characteristic speed; T_c is Combustion chamber temperature; M_c is Average molecular mass of combustion products. All the parameters were calculated by means of software ProPep 3.0 at condition of p_c/p_e=70/1 (p_e=0.1 MPa) and T_0=298 K.

4 Conclusions

In the present paper, the NC/GAP/nano-TATB nanofiber with a 3D net structure is obtained by an electrospinning method. The energetic groups of —ONO_2, —N_3, —NO_2 and —NH_2 are detected on the surface of NC/GAP/nano-TATB nanofibers.

For thermolysis, the NC/GAP/nano-TATB nanofibers decompose at the temperature range of 198~214 ℃. There is only one thermal decomposition peak. The various components of nanofibers play a synergistic role in thermolysis. The E_a of NC/GAP/nano-TATB is 208.124 kJ·mol^{-1}, which is higher than that of NC/GAP. The k of NC/GAP/nano-TATB (1.7 s^{-1}) is hgher than that of nano-TATB (0.92 s^{-1}) and NC/GAP(1.43 s^{-1}). The decomposition products of NC/GAP/nano-TATB include NO, NO_2, N_2O, H_2O, CO and CO_2.

The addition of TATB results in an improvement of combustion chamber temperature (T_c) and average molecular mass of combustion products (M_c). The I_{sp} of NC/GAP/nano-TATB (2000.9 N·s·kg^{-1}) is observably higher than TATB and slightly lower than NC/GAP. M_c play a dominant role in energy performance. The H_{50} of NC/GAP/nano-TATB is up to 90.87 cm, which is higher than that of NC/GAP (59.28 cm). The introduction of TATB reduces the impact sensitivity of NC/GAP. Overall, the NC/GAP/nano-TATB nanofibers possess distinguished energy properties of higher specific impulse and lower impact sensitivity. This paper reveals the preferable application potential in the weapon energy system, especially in the solid rocket-propellant field.

References:

[1] Badgujar D M, Talawar M B, Asthana S N, et al. Advances in science and technology of modern energetic materials: An overview[J]. *Journal of Hazardous Materials*, 2008, 151(2-3): 289-305.

[2] Pagoria P F, Lee G S, Mitchell A R, et al. A review of energetic materials synthesis[J]. *Thermochimica Acta*, 2002, 384 (1-2): 187-204.

[3] Talawar M B, Sivabalan R, Mukundan T, et al. Environmentally compatible next generation green energetic materials (GEMs)[J]. *Journal of Hazardous Materials*, 2009, 161(2-3): 589-607.

[4] Zhou Xiang, Torabi M, Lu Jian, et al. Nanostructured energetic composites: Synthesis, ignition/combustion modeling, and applications[J]. *Acs Applied Materials & Interfaces*, 2014, 6 (5): 3058.

[5] Jadhav H S, Talawar M B, Sivabalan R, et al. Synthesis, characterization and thermolysis studies on new derivatives of 2,4,5-trinitroimidazoles: Potential insensitive high energy materials [J]. *Journal of Hazardous Materials*, 2007, 143 (1-2): 192-197.

[6] King W P, Saxena S, Nelson B A, et al. Nanoscale thermal analysis of an energetic material[J]. *Nano Letters*, 2015, 6 (9): 2145-2149.

[7] Sikder A K, Sikder N. A review of advanced high performance, insensitive and thermally stable energetic materials emerging for military and space applications[J]. *Journal of hazardous materials*, 2004, 112(1-2): 1-15.

[8] Rossi C, Estève A, Vashishta P. Nanoscale energetic materials [J]. *Journal of Physics & Chemistry of Solids*, 2010, 71(2): 57-58.

[9] Reid D L, Russo A E, Carro R V, et al. Nanoscale additives tailor energetic materials[J]. *Nano Letters*, 2007, 7(7): 2157-2161.

[10] Son S F, Yetter R, Yang V. Introduction: Nanoscale composite energetic materials[J]. *Journal of Propulsion & Power*, 2007, 23(4): 643-644.

[11] Bezmelnitsyn A, Thiruvengadathan R, Barizuddin S, et al. Modified nanoenergetic composites with tunable combustion characteristics for propellant applications[J]. *Propellants Explosives Pyrotechnics*, 2010, 35(4): 384-394.

[12] Sundaram D, Yang V, Yetter R A. Metal-based nanoenergetic materials: Synthesis, properties, and applications[J]. *Progress in Energy & Combustion Science*, 2017, 61(2017): 293-365.

[13] Stacy S C, Massad R A, Pantoya M L. Pre-ignition laser ablation of nanocomposite energetic materials[J]. *Journal of Applied Physics*, 2013, 113(21): 213107.

[14] Chen Ren-jie, Luo Yun-jun, Sun Jie, et al. Preparation and properties of an AP/RDX/SiO_2 nanocomposite energetic material by the sol-gel method[J]. *Propellants Explosives Pyrotechnics*. 2012, 37(4): 422-426.

[15] Huang Zheng-ming, Zhang Yan-zhong, Kotaki M, et al. A review on polymer nanofibers by electrospinning and their applications in nanocomposites[J]. *Composites Science & Technology*, 2003, 63(15): 2223-2253.

[16] Bhardwaj N, Kundu S C. A fascinating fiber fabrication technique[J]. *Biotechnology Advances*, 2010, 28(3): 325-347.

[17] Teo W E and Ramakrishna S. A Review on electrospinning design and nanofibre assemblies[J]. *Nanotechnology*, 2006, 17 (14): 89-106.

[18] Andreas G and Wendorff J H. Electrospinning: A fascinating

method for the preparation of ultrathin fibers[J]. *Angewandte Chemie*, 2010, 46(30): 5670-5703.
[19] Agarwal S, Greiner A, Wendorff J H. Functional materials by electrospinning of polymers[J]. *Progress in Polymer Science*, 2013, 38(6): 963-991.
[20] Zhang Chuan-ling, Yu Shu-hong. Spraying functional fibres by electrospinning[J].*Materials Horizons*,2016,3(4): 266-269.
[21] Essalhi M, Khayet M. Self-sustained webs of polyvinylidene fluoride electrospun nanofibers at different electrospinning times: 1. Desalination by direct contact membrane distillation [J].*Journal of Membrane Science*,2013,433(2013): 167-179.
[22] Shi Yang, Guo Qiang-jian, Zachariah M R. Electrospun nanofiber-based thermite textiles and their reactive properties[J]. *Acs Applied Materials & Interfaces*, 2012, 4(12):6432-6435.
[23] Li Yang-chun, Yang Hong-tao, Hong Ying, et al. Electrospun nanofiber-based nanoboron/nitrocellulose composite and their reactive properties[J]. *Journal of Thermal Analysis & Calorimetry*, 2017, 130(4): 1063-1068.
[24] Li Meng-yao, Huang Rong-hui, Yan Shi. Preparation of NC/CL-20 composite fibers by electrospinning [C]//International Workshop on Material Science and Environmental Engineering , 2016:165-172.
[25] You J S, Kweon J O, Kang S C, et al. A kinetic study of thermal decomposition of glycidyl azide polymer (GAP)-based energetic thermoplastic polyurethanes [J]. *Macromolecular Research*, 2010, 18(12): 1226-1232.
[26] Pisharath S, Ang H G. Synthesis and thermal decomposition of GAP-Poly(BAMO) copolymer[J]. *Polymer Degradation & Stability*, 2007, 92(7): 1365-1377.
[27] Ma F O, María L L, Torre M, et al. Analytical techniques in the study of highly-nitrated nitrocellulose [J]. *Trac Trends in Analytical Chemistry*, 2011, 30(11):1740-1755.
[28] LI Guo-ping, Liu Meng-hui, Zhang Ran, et al. Synthesis and properties of RDX/GAP nano-composite energetic materials [J]. *Colloid and Polymer Science*, 2015, 293(8):2269-2279.
[29] Boddu V M, Viswanath D S, Ghosh T K, et al. 2,4,6-Triamino-1, 3, 5-trinitrobenzene (TATB) and TATB-based formulations—A review [J]. *Journal of Hazardous Materials*, 2010, 181(1-3):1-8.
[30] Huang Bing, Hao Xiao-fei, Zhang Hao-bin, et al. Ultrasonic approach to the synthesis of HMX@TATB core-shell microparticles with improved mechanical sensitivity[J]. *Ultrasonics Sonochemistry*, 2014, 21(4):1349-1357.
[31] Yoshihara K, Tanaka A. Interlaboratory study on the degradation of poly(vinyl chloride), nitrocellulose and poly(tetrafluoroethylene) by x-rays in XPS[J]. *Surface and Interface Analysis*, 2002, 33(3):252-258.
[32] Shin W G, Han D, Park Y, et al. Combustion of boron particles coated with an energetic polymer material [J]. *Korean Journal of Chemical Engineering*, 2016, 33(10):3016-3020.
[33] MA Xiao-jing, Elbohy H, Sigdel S. Electrospun carbon nano-felt derived from alkali lignin for cost-effective counter electrodes of dye-sensitized solar cells[J]. *RSC Adv*, 2016, 6(14): 11481-11487.
[34] Ding Bin, Kim H, Kim C, et al. Morphology and crystalline phase study of electrospun TiO_2-SiO_2 nanofibres[J]. *Nanotechnology*, 2003, 14(5): 532.
[35] Wang Yi, Song Xiao-lan, Song Dan, et al. Synthesis, thermolysis, and sensitivities of HMX/NC energetic nanocomposites [J]. *Journal of Hazardous Materials*,2016,312(2016): 73-83.
[36] Sovizi M R, Hajimirsadeghi S S, Naderizadeh B. Effect of particle size on thermal decomposition of nitrocellulose[J]. *Journal of Hazardous Materials*, 2009, 168(2-3): 1134-1139.
[37] Wang Yi, Zhang Mi, Song Xiao-lan, et al. Characteristics and properties of nitrocellulose/glycidyl azide polymer/2, 4, 6, 8, 10,12-hexanitro-2,4,6,8,10,12-hexaazaisowurtzitane nanocomposites synthesized using a sol-gel supercritical method [J]. *Nanomater. Nanotechno*, 2019, 9(3): 1-12.
[38] Wang Yi, Song Xiao-lan, Li Feng-sheng. Thermal behavior and decomposition mechanism of ammonium perchlorate and ammonium nitrate in the presence of nanometer triaminoguanidine nitrate[J]. *ACS Omega*,2019,4(1): 214-225.

3D网状静电纺NC/GAP/nano-TATB纤维的表征及热化学性能

罗婷婷[1],王 毅[1],刘丽霞[2],宋小兰[3]

(1.中北大学材料科学与工程学院, 山西 太原 030051; 2.北方爆破技术有限公司阳泉分公司, 山西 阳泉 045000; 3.中北大学环境与安全工程学院, 山西 太原 030051)

摘 要: 采用静电纺丝法制备了具有三维网络结构的硝化纤维素/聚叠氮缩水甘油醚/三氨基三硝基苯(NC/GAP/nano-TATB)复合纤维。采用差示扫描量热法(DSC)和热红外法(TG-IR)对复合纤维的低温热化学性能进行了研究。结果显示,每条曲线上只有一个放热峰,,NC、GAP和nano-TATB同时分解,而非单独分解。NC/GAP/nano-TATB(208.1 kJ·mol^{-1})的活化能(E_a)低于nano-TATB(228.9 kJ·mol^{-1}),NC/GAP/nano-TATB (1.70 s^{-1})的速率常数(k)高于nano-TATB(0.92 s^{-1})。复合纤维比纳米TATB更容易被活化,分解速度更快。NC/GAP/nano-TATB热分解的主要产物为CO_2、N_2O、NO、CO、NO_2、H_2O,同时检测到—CH—、—CH_2O、—C—O—C—片段。对比了复合纤维和NC/GAP和nano-TATB的能量和敏感性。NC/GAP/nano-TATB的燃烧室温度(T_c)高达1583℃,纳米TATB的加入有利于降低冲击敏感度。

关键词: 静电纺丝;纤维素/聚叠氮缩水甘油醚/三氨基三硝基苯(NC/GAP/nano-TATB);热分解;能量性能;敏感度

中图分类号: TJ55; O649 **文献标志码:** A **DOI:**10.11943/CJEM2019283

(责编:高 毅)